

1 Northern Sourced Water dominated the Atlantic Ocean during the
2 Last Glacial Maximum

3 **F. Pöppelmeier¹, P. Blaser¹, M. Gutjahr², S. L. Jaccard³, M. Frank², L. Max⁴, J. Lippold¹**

4 *¹Institute of Earth Sciences, Heidelberg University, 69120 Heidelberg, Germany*

5 *²GEOMAR Helmholtz Center for Ocean Research Kiel, 24148 Kiel, Germany*

6 *³Institute of Geological Sciences and Oeschger Center for Climate Change Research, University of
7 Bern, 3012 Bern, Switzerland*

8 *⁴MARUM-Center for Marine Environmental Sciences, University of Bremen, 28359 Bremen,
9 Germany*

10 **ABSTRACT**

11 Increased carbon sequestration in the ocean subsurface is commonly assumed to have been
12 one of the main causes responsible for lower glacial atmospheric CO₂ concentrations.
13 Remineralized carbon must have been stored away from the atmosphere for thousands of years, yet
14 the water mass structure accommodating such increased carbon storage continues to be debated.
15 Here we present new sediment derived bottom water neodymium isotope records that allow
16 fingerprinting of water masses and provide a more complete picture of the Atlantic overturning
17 circulation geometry during the Last Glacial Maximum. These results suggest that the vertical and
18 meridional structure of the Atlantic water mass distribution only experienced minor changes since
19 the last ice age. In particular, we find no compelling evidence supporting glacial southern sourced
20 water substantially expanding to shallower depths and farther into the northern hemisphere than
21 today, which has been previously inferred from stable carbon isotope ($\delta^{13}\text{C}$) reconstructions. We
22 argue that depleted $\delta^{13}\text{C}$ values observed in the deep Northwest Atlantic do not necessarily indicate
23 the presence of southern sourced water. Instead, these values may represent a northern sourced
24 water mass with lower than modern preformed $\delta^{13}\text{C}$ values that were further modified downstream
25 by increased sequestration of remineralized carbon, facilitated by a more sluggish glacial deep
26 circulation corroborating previous evidence.

27 **INTRODUCTION**

28 During the Last Glacial Maximum (LGM) atmospheric CO₂ concentrations were ~90 ppm
29 lower than during pre-industrial times (Monnin et al., 2001). Converging evidence suggests that a
30 considerable amount of remineralized CO₂ was sequestered from the atmosphere into the deep
31 ocean due to an overall more efficient biological carbon pump, a more stratified Southern Ocean,
32 and globally lower sea surface temperatures increasing the solubility of CO₂ (Broecker, 1982;
33 Galbraith and Jaccard, 2015). Further, it has been proposed that enhanced oceanic CO₂ storage was

34 facilitated by stronger deep water stratification along with increased ocean alkalinity (Broecker and
35 Peng, 1989). Benthic foraminiferal carbon isotope-based reconstructions ($\delta^{13}\text{C}$ and $\Delta^{14}\text{C}$) of the
36 Atlantic Meridional Overturning Circulation (AMOC) support the notion of an enhanced glacial
37 deep ocean stratification by indicating that young, nutrient-rich waters occupied water depths
38 shallower than ~ 2500 m, whereas older, nutrient depleted waters prevailed below (Curry and Oppo,
39 2005). The similarity of LGM deep North Atlantic carbon isotope compositions to those of glacial
40 North Pacific Deep Water led to the suggestion that large parts of the glacial deep Atlantic were
41 filled with Southern Sourced Water (SSW; Curry and Oppo, 2005; Keigwin, 2004). Such a
42 circulation pattern differs fundamentally from the modern AMOC geometry, in which SSW
43 advection is mostly confined to the deep Southwest Atlantic (Fig. 1). However, a major caveat of
44 carbon isotope based paleoceanographic reconstructions is their inherent dependency on changes in
45 the carbon cycle. For instance, the stable carbon isotope ($\delta^{13}\text{C}$) distribution of dissolved inorganic
46 carbon reflects water mass provenance, but remineralization of organic matter can substantially alter
47 the $\delta^{13}\text{C}$ signature of a water mass independent of mixing (Lynch-Stieglitz et al., 2007).
48 Furthermore, $\delta^{13}\text{C}$ as well as $\Delta^{14}\text{C}$, are influenced by changes in air-sea carbon exchange (Broecker
49 and Maier-Reimer, 1992). Thus, distinguishing water mass provenance from carbon cycle related
50 changes constitutes a major difficulty intrinsic to these proxies.

51 The radiogenic neodymium isotopic signature (ϵNd), independent of the carbon cycle, is a
52 promising proxy that behaves quasi-conservatively in the Atlantic Ocean (van de Flierdt et al.,
53 2016). In the modern Atlantic, Northern Sourced Water (NSW) is characterized by a dissolved Nd
54 isotope signature of -12.8 ± 0.4 whereas SSW has a distinctly more radiogenic (higher) signature of
55 -9.0 ± 0.4 (Stichel et al., 2012). However, these ϵNd end members were not constant through time.
56 During the LGM SSW exhibited higher values around -5.5 (Skinner et al., 2013), likely due to the
57 absence of bottom water export from the Weddell Sea into the Atlantic as recently reported by
58 Huang et al. (2020). Similarly, new reconstructions of the northern end member indicate a higher

59 glacial ϵ Nd value between -10 and -11 of NSW at 40°N (Zhao et al., 2019). The authors argue that
60 the unradiogenic Canadian Shield and Greenland contributed considerably less Nd to the North
61 Atlantic during the LGM, due to extensive ice-sheet cover of these provinces. Consideration of
62 these ϵ Nd end members allows for a more accurate interpretation of past changes in water mass
63 distribution of the Atlantic.

64 Here we present new Nd isotope reconstructions that close a crucial data gap in the deep
65 Southwest Atlantic. We combine these new data with published time series from the West Atlantic
66 (Howe et al., 2016; Pöppelmeier et al., 2020; Skinner et al., 2013) to generate transects for the late
67 Holocene and LGM time slices. Building on the compilation of Howe et al. (2016), we further
68 reconstruct the vertical water mass structure at 30°S in high resolution, assess the potential
69 influence of benthic exchange processes on bottom water ϵ Nd by employing a box model, and by
70 excluding regions where such processes are exacerbated by benthic nepheloid layers (Northwest
71 Atlantic and Cape Basin, Pöppelmeier et al., 2019). Hence, we are able to robustly reconstruct
72 glacial-interglacial changes of the deep water geometry.

73 **METHODS**

74 Authigenic Nd was extracted from bulk sediment following the protocol of Blaser et al.
75 (2016). The Nd isotopic compositions were measured on two Neptune Plus MC-ICP-MSs at
76 GEOMAR, Kiel and the University of Erlangen-Nuernberg, Germany. Instrumental mass
77 fractionation was corrected for by normalizing $^{146}\text{Nd}/^{144}\text{Nd}$ to 0.7219. Further, samples were
78 bracketed by JNdi-1 standard reference solution normalized to the accepted value of $^{143}\text{Nd}/^{144}\text{Nd} =$
79 0.512115 (Tanaka et al., 2000). The external reproducibility (2σ) was determined by repeated in-
80 house standard measurements and varied between 0.12 and 0.50 ϵ -units in different sessions.

81 RESULTS AND DISCUSSION

82 The spatial distribution of sediment core data is arguably sparse compared to modern
83 oceanographic seawater sampling stations. To nonetheless allow for a comparison between
84 Holocene-aged ϵNd reconstructions and modern oceanography and water mass provenance, we
85 choose the 4000 ± 500 m water depth isobath to derive the relative proportion of SSW at a given
86 location based on modern oceanographic parameters (silicate, N^* , pot. T, and salinity; Figs. 1A and
87 S1) and compare to core-top measurements at similar depths. This water depth represents the lower
88 limit up to which well dated sediment cores are available in sufficient quantity, as robustly dating
89 sediments from greater depths becomes increasingly difficult due to poor preservation of calcium
90 carbonate and generally lower sedimentation rates (Broecker, 1982).

91 To calculate the proportion of SSW based on the ϵNd reconstructions, we used a binary
92 mixing model with modern seawater compositions (van de Flierdt et al., 2016) and reconstructed
93 (Huang et al., 2020; Zhao et al., 2019) end members for the Holocene and LGM, respectively. At
94 the 4000 m isobath late Holocene ϵNd based reconstructions and modern oceanography both show a
95 coherent decrease of SSW from nearly 100% at 45°S to less than 20% north of the Equator (i.e.
96 $\Delta\text{SSW} \approx 85\%$, Fig. 2A), which supports the validity of the Nd isotope proxy as a semi-conservative
97 water mass tracer along the transect. Based on ϵNd reconstructions this meridional water mass
98 gradient existed with nearly the same configuration during the LGM (Fig. 2B), with a decrease of
99 the SSW proportion from 100% at 45°S to about 20% north of the Equator ($\Delta\text{SSW} \approx 80\%$). For
100 these calculations we consider Nd concentrations as constant due to a lack of observational data, but
101 moderate variations of modern Nd concentrations do not lead to changes in our interpretations (Fig.
102 S5). Such a sharp meridional deep water mass gradient strongly contrasts with nutrient proxies that
103 suggest a substantially greater amount of SSW bathing large parts of the deep North Atlantic basin
104 during the LGM (Curry and Oppo, 2005). This discrepancy raises the question whether the Nd
105 isotope derived water mass gradient is at least partly affected by non-conservative processes.

106 Benthic Nd addition represents the main process capable of altering the Nd isotopic composition of
107 bottom waters independent of water mass mixing (Haley et al., 2017). To quantitatively test the
108 influence of a potential benthic Nd source on the observed ϵNd gradient of the LGM we employ a
109 simple box model (Fig. S6). In the model, we only consider the flow path between the Rio Grande
110 Rise and the Equatorial Atlantic, because ϵNd reconstructions farther south show a homogeneous
111 signal. This is a first indication that basin-wide benthic Nd addition only played a subordinate role.
112 The reasoning for this is that a strong benthic flux would produce an ϵNd gradient along the flow
113 path of SSW, assuming that the signature matched not exactly the initial bottom water ϵNd value,
114 which is not observed here. For conservative parameter estimates of the advection rate and benthic
115 Nd flux (<4 Sv and $30 \text{ pmol/cm}^2/\text{year}$ (Abbott et al., 2015) and $\epsilon\text{Nd}_{\text{detrital}} = -7$ (Pöppelmeier et al.,
116 2020), respectively) the model results suggest that non-conservative benthic Nd addition may have
117 produced about 0.5 ϵ -units of the total meridional ~ 4.5 ϵ -units gradient, which translates into a
118 negligible decrease of the SSW gradient (from $\Delta\text{SSW} \approx 80\%$ to $\sim 75\%$; Fig. S8). Even for an
119 unrealistically, extreme scenario that this non-conservative process contributed 2 of the 4.5 ϵ -units
120 meridional Nd isotope gradient (< 2 Sv and $\epsilon\text{Nd}_{\text{detrital}} = -10$), the decrease in the SSW gradient
121 amounts to only about 10% (from $\Delta\text{SSW} \approx 80\%$ to $\sim 70\%$). Thus, we conclude that the meridional
122 gradient in past bottom water Nd isotopes is robust, which implies dominance of NSW over SSW in
123 the glacial deep Equatorial and North Atlantic.

124 In order to not only constrain the latitudinal spread of glacial SSW but also the vertical
125 extent of this water mass, we reconstructed past seawater ϵNd for a depth transect near 30°S (Figs.
126 3). In this region, the modern water mass boundary between SSW and NSW is situated at depths
127 between 3500 and 4000 m (as defined by the 50% mixing ratio (Fig. 1A)). Modern seawater and
128 reconstructed Holocene ϵNd data capture this feature well. During the LGM the Nd isotope data
129 were generally more radiogenic than modern, due to the more radiogenic end members, but at
130 ~ 3500 m water depth a sharp 2.5 ϵ -units step is observed. Since the investigated sites are not only

131 located at the continental margin but are also in pelagic environments (Fig. 1B), local detrital input
132 effects cannot account for the observed ϵNd depth trend, but instead must represent a more
133 integrated regional signal. Therefore, the most plausible explanation for the marked ϵNd gradient at
134 ~ 3500 m is the presence of a pronounced water mass boundary between NSW (less radiogenic)
135 above and SSW (more radiogenic) below. Since non-conservative processes cannot account for the
136 meridional and vertical ϵNd gradients observed here, the data clearly indicate that similar to modern
137 proportions of NSW bathed the entire deep Northwest Atlantic during the LGM. This calls into
138 question the nutrient-proxy based interpretation of a glacial deep Atlantic dominated by SSW.

139 Stable carbon isotope reconstructions have a long-standing history as a water mass tracer
140 and a recent study confirmed the good correlation between core top and seawater $\delta^{13}\text{C}$ on a global
141 scale (Schmittner et al., 2017). However, Holocene-aged core top reconstructions in key regions
142 such as the deep Northwest Atlantic partly deviate from seawater $\delta^{13}\text{C}$, potentially related to the
143 regionally elevated accumulation of organic matter (Fig. S8, Keigwin, 2004). $\delta^{13}\text{C}$ reconstructions
144 from sites that exhibit these core top – seawater offsets have also been used for interpretation of
145 past seawater provenance (Keigwin, 2004). $\delta^{13}\text{C}$ signatures at these sites have been interpreted as
146 high SSW contributions during the LGM (Keigwin, 2004), which may at least partly be biased by
147 the same obfuscating effects that produce the core top – seawater offset at these locations today.
148 Furthermore, model simulations suggest that the shoaling of NSW, previously inferred from
149 nutrient-like proxies, may have been limited to the core of the water mass (defined as the depth with
150 the strongest advection) and may not have affected the boundary between NSW and SSW to the
151 same extent (Gebbie, 2014; Oppo et al., 2018). Yet ocean circulation models are inconsistent on this
152 issue, with roughly half of the models within the Paleoclimate Model Intercomparison Project 2
153 (PMIP2) showing a shallower NSW while the others yield deep NSW during the LGM comparable
154 to the modern geometry (Weber et al., 2007). On the other hand, the majority of models in the later
155 PMIP3 favor a circulation pattern similar to modern (Muglia and Schmittner, 2015). One possibility

156 to reconcile a modern-like extent of NSW in the Northwest Atlantic with the observed ^{13}C
157 depletions relates to increased accumulation of respired carbon originating from remineralization of
158 organic matter (Gebbie, 2014). This remineralization may have been facilitated or amplified by the
159 less vigorous Atlantic deep water circulation of the LGM as indicated by Pa/Th (McManus et al.,
160 2004; Ng et al., 2018) and generally colder ocean temperatures (Matsumoto, 2007). Likewise, ^{14}C
161 data suggest a higher ventilation age of the deep Atlantic during the LGM allowing for deep water
162 to accumulate more respired carbon and thus lowering its $\delta^{13}\text{C}$ signature (Skinner et al., 2017). In
163 addition, these ^{14}C data show aging of deep waters from North to South as expected from a deep
164 northern sourced water mass propagating southward.

165 These consistent observations lead us to the conclusion that the glacial deep water mass
166 distribution was not substantially different from today (Fig. 4). Our new Nd isotope reconstructions
167 suggest that glacial SSW may have penetrated slightly farther northward than today, but was still
168 mostly confined to the deep South Atlantic with a vertical expansion similar to the modern Atlantic.
169 Thus, as a direct consequence, NSW must have dominated the deep North Atlantic also with a
170 spatial expansion similar to today. We hence argue that the shallower stratification observed in the
171 North Atlantic with nutrient-based proxies was instead likely the result of differences in the
172 contribution of remineralized organic matter to the upper and lower limb of NSW due to different
173 advection rates of both limbs (Ng et al., 2018; Skinner et al., 2017). This is in accordance with the
174 rather steady change of $\delta^{13}\text{C}$ with depth that do not indicate a clear water mass boundary (Fig. S10).
175 Since Nd is not affected by biological cycling, this chemical divide did not affect the ϵNd
176 distribution. The deep Atlantic-wide evidence for elevated deep water Pa/Th (Ng et al., 2018) and
177 the prolonged glacial deep-to-surface supply of Southern Ocean waters (Hasenfratz et al., 2019)
178 nevertheless suggests LGM circulation modes substantially different from the Holocene situation.

179 **ACKNOWLEDGMENTS**

180 We thank Marcel Regelous for technical help and Delia Oppo for fruitful discussions. Samples were
181 provided by the WHOI core repository and the GeoB core repository at MARUM, University of
182 Bremen. Financial support for this research was provided by the Emmy-Noether Programme of the
183 DFG through grant Li1815/4. SLJ acknowledges support from the SNSF (grant PP00P2_172915).

184 **REFERENCES CITED**

- 185 Abbott, A. N., Haley, B. A., and McManus, J. (2015). Bottoms up: Sedimentary control of the deep
186 North Pacific Ocean's ϵNd signature. *Geology* v. 43, p. 1035-1038. doi:10.1130/G37114.1
- 187 Blaser, P., Lippold, J., Gutjahr, M., Frank, N., Link, J. M., & Frank, M. (2016). Extracting
188 foraminiferal Nd isotope signatures from bulk deep sea sediment by chemical leaching.
189 *Chemical Geology* v. 439, p. 189–204. doi:10.1016/j.chemgeo.2016.06.024
- 190 Broecker, W. S. (1982). Glacial to interglacial changes in ocean chemistry. *Progress in*
191 *Oceanography* v. 11(2), p. 151-197. doi:10.1016/0079-6611(82)90007-6
- 192 Broecker, W. S., & Maier-Reimer, E. (1992). The influence of air and sea exchange on the carbon
193 isotope distribution in the sea. *Global Biogeochemical Cycles* v. 6 (3), p. 315-320.
194 doi:10.1029/92GB01672
- 195 Broecker, W. S., and Peng, T.-H. (1989). The cause of the glacial to interglacial atmospheric CO_2
196 change: A polar alkalinity hypothesis. *Global Biogeochemical Cycles* v.3, p. 215-239.
197 doi:10.1029/GB003i003p00215
- 198 Curry, W. B., & Oppo, D. W. (2005). Glacial water mass geometry and the distribution of $\delta^{13}\text{C}$ of
199 CO_2 in the western Atlantic ocean. *Paleoceanography* v. 20 (1). doi:10.1029/2004PA001021

- 200 Galbraith, E. D., & Jaccard, S. L. (2015). Deglacial weakening of the oceanic soft tissue pump:
201 Global constraints from sedimentary nitrogen isotopes and oxygenation proxies. *Quaternary*
202 *Science Reviews* v. 109, p. 38-48. doi:10.1016/j.quascirev.2014.11.012
- 203 Gebbie, G. (2014). How much did Glacial North Atlantic Water shoal? *Paleoceanography* v. 29, p.
204 190-209. doi:10.1002/2013PA002557
- 205 Gutjahr, M., Frank, M., Stirling, C. H., Keigwin, L. D., & Halliday, A. N. (2008). Tracing the Nd
206 isotope evolution of North Atlantic deep and intermediate waters in the western North
207 Atlantic since the Last Glacial Maximum from Blake Ridge sediments. *Earth and Planetary*
208 *Science Letters* v. 266 (1–2), p. 61–77. doi:10.1016/j.epsl.2007.10.037
- 209 Haley, B. A., Du, J., Abbott, A. N., & McManus, J. (2017). The impact of benthic processes on Rare
210 Earth Elements and neodymium isotope distributions in the oceans. *Frontiers in marine*
211 *Science* v. 4:426. doi:10.3389/fmars.2017.00426
- 212 Hasenfratz, A. P. et al. (2019). The residence time of Southern Ocean surface waters and the
213 100,000-year ice age cycle. *Science* v. 363, p. 1080-1084. doi:10.1126/science.aat7067
- 214 Howe, J. N. W., Piotrowski, A. M., Noble, T. L., Mulitza, S., Chiessi, C. M., & Bayon, G. (2016).
215 North Atlantic deep water production during the Last Glacial Maximum. *Nature*
216 *Communications* v. 7:11765. doi:10.1038/ncomms11765
- 217 Huang, H., Gutjahr, M., Eisenhauer, A., & Kuhn, G. (2020). No detectable Weddell Sea Antarctic
218 Bottom Water export during the Last and Penultimate Glacial Maximum. *Nature*
219 *Communication* v. 11:424. doi:10.1038/s41467-020-14302-3
- 220 Jeandel, C. (1993). Concentrations and isotopic compositions of Nd in the South Atlantic Ocean.
221 *Earth and Planetary Science Letters* v. 117, p. 581-591. doi:10.1016/0012-821x(93)90104-h

- 222 Keigwin, L. D. (2004). Radiocarbon and stable isotope constraints on Last Glacial Maximum and
223 Younger Dryas ventilation in the western North Atlantic. *Paleoceanography* v. 19 (4), p. 1–
224 15. doi:10.1029/2004PA001029
- 225 Lynch-Stieglitz, J. et al. (2007). Atlantic Meridional Overturning Circulation during the Last Glacial
226 Maximum. *Science* v. 316, p. 66-69. doi:10.1126/science.1137127
- 227 Matsumoto, K. (2007). Biology-mediated temperature control on atmospheric pCO₂ and ocean
228 biogeochemistry. *Geophysical Research Letters* v. 34. doi:10.1029/2007GL031301
- 229 McManus, J. F., Francois, R., Gherardi, J.-M., Keigwin, L. D., & Brown-Leger, S. (2004). Collapse
230 and rapid resumption of Atlantic meridional circulation linked to deglacial climate changes.
231 *Nature* v. 428 (6985), p. 834–837. doi:10.1038/nature02494
- 232 Monnin, E., Indermühle, A., Dällenbach, A., Flückiger, J., Stauffer, B., Stocker, T. F., Raynaud, D.,
233 and Barnola, J.-M. (2001). Atmospheric CO₂ concentrations over the Last Glacial
234 Termination. *Science* v. 291, p. 112-115. doi:10.1126/science.291.5501.112
- 235 Muglia, J. & Schmittner, A. (2015). Glacial Atlantic overturning increased by wind stress in climate
236 models. *Geophysical Research Letters* v. 42, p.9862-9869. doi:10.1002/2015GL064583
- 237 Ng., H. C., et al. (2018). Coherent deglacial changes in western Atlantic Ocean circulation. *Nature*
238 *Communications* v. 9:2947. doi:10.1038/s41467-018-05312-3
- 239 Oppo, D. W., Gebbie, G., Huang, K.-F., Curry, W. B., Marchitto, T. M., & Pietro, K. R. (2018). Data
240 constraints on glacial Atlantic water mass geometry and properties. *Paleoceanography and*
241 *Paleoclimatology* v. 33:9, p. 1013-1034. doi:10.1029/2018PA003408
- 242 Pöppelmeier, F., Blaser, P., Gutjahr, M., Sufke, F., Thornalley, D. J. R., Grützner, J., Jakob, K. A.,
243 Link, J. M., Szidat, S., Lippold, J. (2019). Influence of ocean circulation and benthic
244 exchange on deep Northwest Atlantic Nd isotope records during the past 30,000 years.
245 *Geochemistry, Geophysics, Geosystems*, v. 20, p. 4457-4469. doi:10.1029/2019GC008271

246 Pöppelmeier, F., Gutjahr, M., Blaser, P., Oppo, D. W., Jaccard, S. L., Regelous, M., Huang, K.-F.,
247 Süfke, F., Lippold, J. (2020). Water mass gradients of the mid-depth Southwest Atlantic
248 during the past 25,000 years. *Earth and Planetary Science Letters* v. 531,
249 doi:10.1016/j.epsl.2019.115963 .

250 Schlitzer, R., et al. (2018). The GEOTRACES intermediate data product 2017. *Chemical Geology* v.
251 493, p. 210-223. doi:10.1016/j.chemgeo.2018.05.040

252 Schmittner, A., et al. (2017). Calibration of the carbon isotope composition ($\delta^{13}\text{C}$) of benthic
253 foraminifera. *Paleoceanography* v. 32, p. 512-530. doi:10.1002/2016PA003072

254 Skinner, L. C., et al. (2017). Radiocarbon constraints on the glacial ocean circulation and its impact
255 on atmospheric CO_2 . *Nature Communications* v. 8, p. 1-10. doi:10.1038/ncomms16010

256 Skinner, L. C., Scrivner, A. E., Vance, D., Barker, S., Fallon, S., & Waelbroeck, C. (2013). North
257 Atlantic versus Southern Ocean contribution to a deglacial surge in deep ocean ventilation.
258 *Geology* v. 41 (6), p. 667-670. doi:10.1130/G34133.1

259 Stichel, T., Frank, M., Rickli, J., Haley, B. A. (2012). The hafnium and neodymium isotope
260 composition of seawater in the Atlantic sector of the Southern Ocean. *Earth and Planetary
261 Science Letters* v. 317-318, p. 282-294. doi:10.1016/j.epsl.2014.12.008

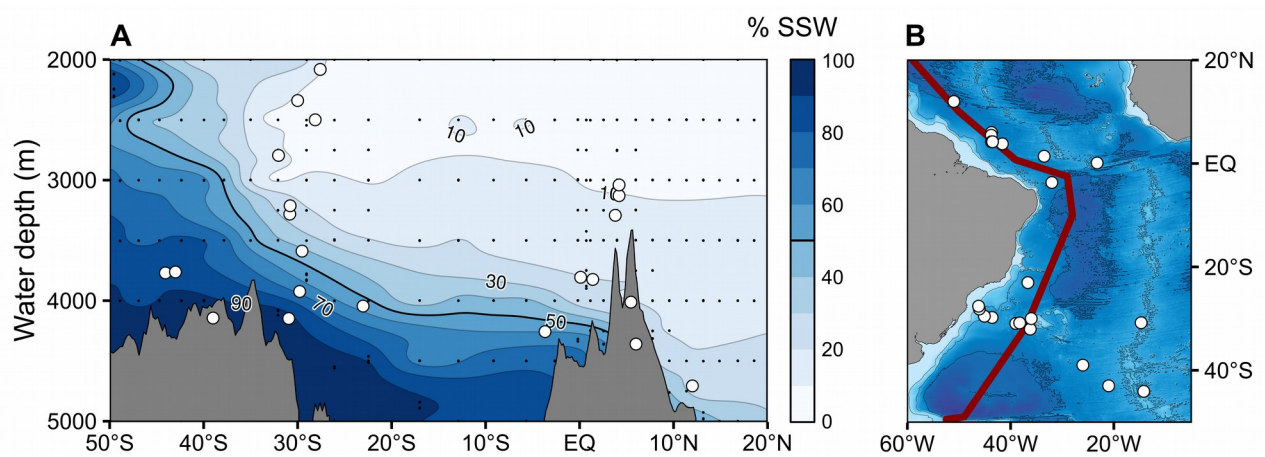
262 Tanaka, T., Togashi, S., Kamioka, H., Amakawa, H., Kagami, H., Hamamoto, T., et al. (2000). JNdi-
263 1: A neodymium isotopic reference in consistency with LaJolla neodymium. *Chemical
264 Geology* v. 168 (3-4), p. 279-281. doi:10.1016/S0009-2541(00)00198-4

265 van de Flierdt, T., Griffiths, A. M., Lambelet, M., Little, S. H., Stichel, T., Wilson, D. J. (2016).
266 Neodymium in the oceans: a global database, a regional comparison and implications for
267 palaeoceanographic research. *Philosophical Transactions A* v. 374 (2081).
268 doi:10.1098/rsta.2015.0293

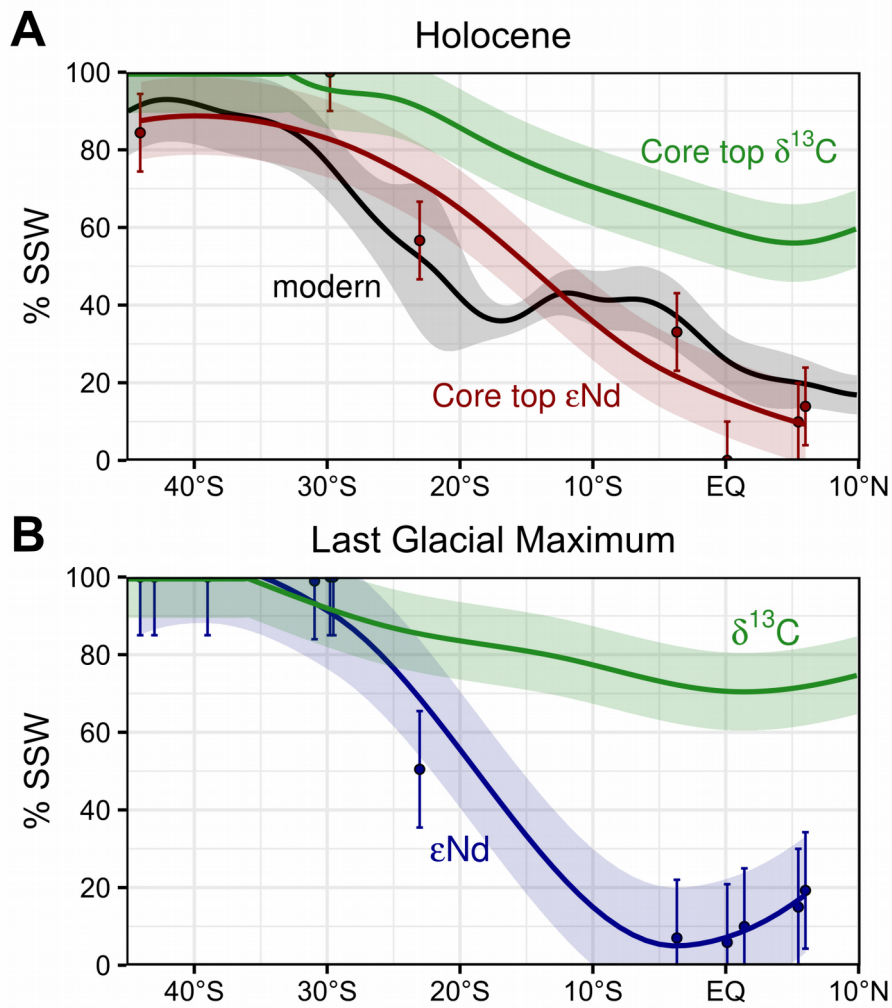
269 Weber, S. L., et al. (2007). The modern and glacial overturning circulation in the Atlantic ocean in
270 PMIP couples model simulations. *Climate of the Past* v. 3, p. 51-64. doi:10.5194/cp-3-51-
271 2007

272 Zhao, N., Oppo, D. W., Huang, K.-F., Howe, J. N. W., Blusztajn, J., & Keigwin L. D. (2019).
273 Glacial–interglacial Nd isotope variability of North Atlantic Deep Water modulated by
274 North American ice sheet. *Nature Communications* v. 10:5773. doi:10.1038/s41467-019-
275 13707-z

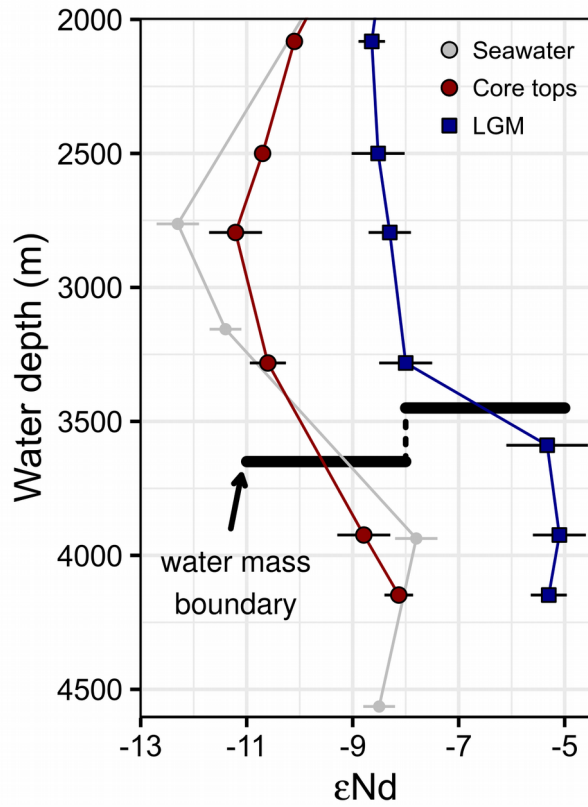
276



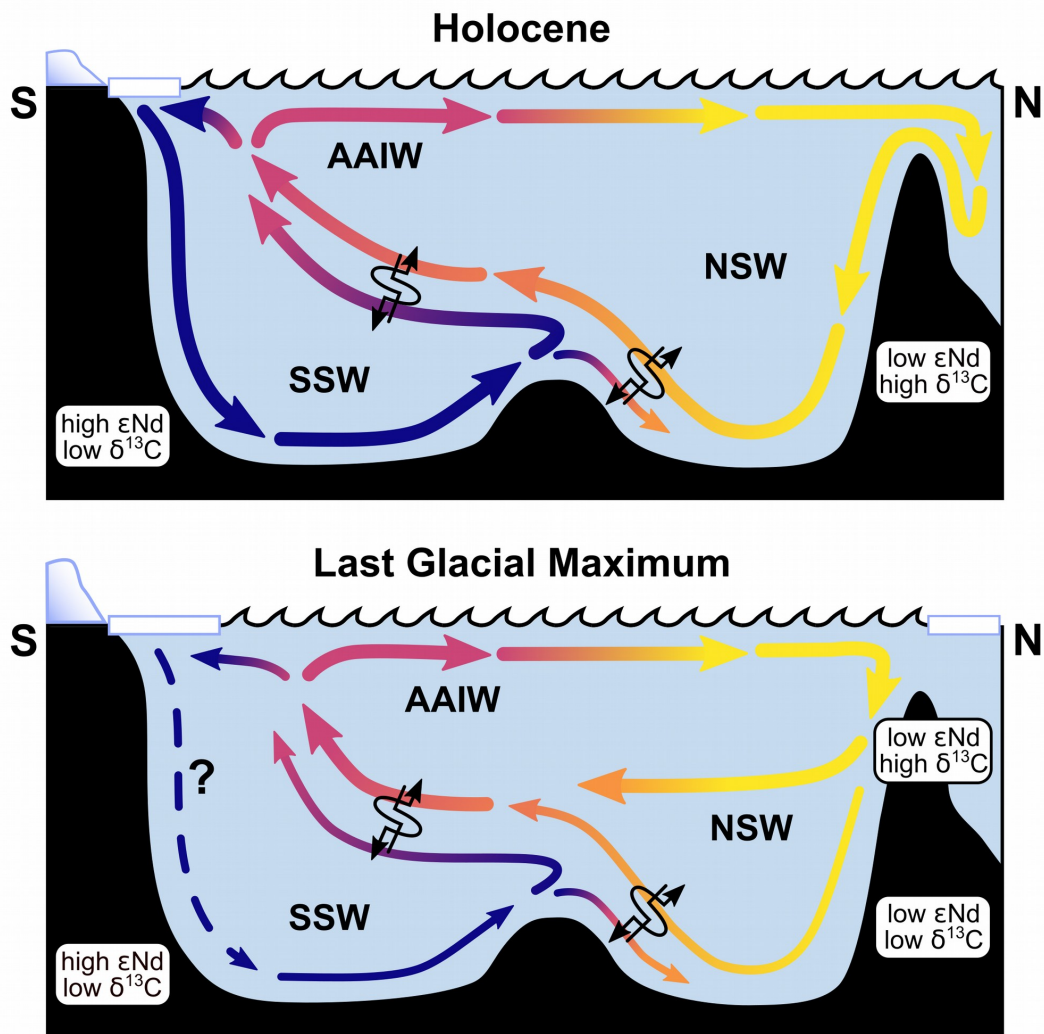
277 Figure 1. (A) Water mass distribution based on four independent conservative water mass properties
278 (Fig. S1) along the GEOTRACES GA02 transect (Schlitzer et al., 2018; red line in panel b). Black
279 dots indicate water sampling stations. (B) Overview map of the tropical and South Atlantic. The red
280 line marks the GA02 transect. Sediment core sites used in this study are marked by open circles in
281 both panels.



282 Figure 2. Deep water provenance of SSW at 4000 ± 500 m water depth. (A) Modern and Holocene
 283 SSW contribution. Black line depicts % SSW at 4000 m derived from modern oceanographic
 284 properties of Fig. 1A. The ϵNd based reconstructions (red line) are Holocene averages of the time
 285 period from 0 to 6.5 ka. $\delta^{13}\text{C}$ data are based on Schmittner et al. (2017) (B) ϵNd based
 286 reconstruction of the deep water mass provenance during the LGM with adjusted end member
 287 compositions. $\delta^{13}\text{C}$ data are based on Oppo et al. (2018). Ribbons depict the uncertainty estimated to
 288 $\pm 10\%$ for the Holocene ϵNd reconstructions and $\pm 15\%$ for the LGM (SI). The uncertainty of the
 289 modern hydrography (panel a, black line) is the 1σ deviation of the calculation for Fig. 1A.



290 Figure 3. ϵNd depth gradient at $\sim 30^\circ\text{S}$. Core tops, representative of the mid to late Holocene are
 291 depicted in red, modern seawater (Jeandel, 1993) in gray, and averaged LGM values in blue. Core
 292 sites are from the Brazil Margin as well as the open ocean (near the Rio Grande Rise). The modern
 293 water mass boundary is derived from the 50% mixing line at 30°S of Fig. 1A.



294 Figure 4. The Holocene overturning (top) shows two main circulation cells, with NSW forming in
 295 the Nordic Seas and Labrador Sea and SSW forming near Antarctica. During the Last Glacial
 296 Maximum (bottom) the proposed circulation scheme consisted of three cells. The reduced deep
 297 water formation in the Nordic Seas produced less deep water and an intermediate depth northern
 298 sourced water mass formed (Glacial North Atlantic Intermediate Water) but at the same time the
 299 formation of SSW was also reduced. The width of the arrows roughly corresponds to proposed
 300 volume transports.

301

302 ¹GSA Data Repository item 201Xxxx, Southwest Atlantic hydrography; sample sites and
303 neodymium isotope data; estimates of benthic flux influence, is available online at
304 www.geosociety.org/pubs/ft20XX.htm, or on request from editing@geosociety.org.